JMEPEG (2003) 12:183-189

A Numerical Analysis of Ceramics Strength Affected by Material Microstructure

Toshihiko Hoshide and Masahiro Okawa

(Submitted 24 August 2001)

To clarify microstructural influences on the ceramic strength, a numerical analysis of the elastic stress distribution around the crack tip for several crack lengths was conducted by using a finite element method (FEM), in which each element was regarded as one grain in a ceramic polycrystal. In the analysis, the anisotropy expected in actual grains was dealt with by randomly assigning different values to the rigidity and the size of each element (i.e., each grain). The FEM results showed that the crack tip stress was dependent on the grain rigidity but was hardly affected by the grain size. A microstructural modification factor f_M for the stress intensity factor was newly introduced to reflect microstructural influences on ceramic strength. The factor f_M was defined as the ratio of the crack tip stress obtained by the FEM analysis to the *K*-based stress. Statistical aspects of f_M were investigated by generating virtual materials with different combinations of grain rigidity and size. When the f_M distribution was fitted to the two-parameter Weibull distribution function, it was clarified that the distribution shifted toward a lower side with increasing the crack length. The *R*-curve expressed by an exponential form was applied so that the grain bridging effect in ceramics could be included in the analysis of the strength depending on crack length. It was revealed that the estimated scatter band in the relation of the strength versus the crack length represented the central trend of dispersed experimental results.

Keywords ceramics, fracture mechanics, microstructure, simulation, strength, small flaw

1. Introduction

It is generally recognized that the brittle fracture of engineering ceramics is dominated by inherent flaws, which are generated during manufacturing. The strength evaluation method based on linear elastic fracture mechanics is usually applied to such a fracture problem. However, when the constant fracture toughness criterion for long cracks is adopted, the strength estimated from the size of the flaw, which is identified as a fracture origin on a fracture surface, is found to be lower than the actual strength observed experimentally.[1-8] There is a possibility that the fracture criterion based on the stress intensity factor *K*, which is effective for cracks with the size enough larger than material microstructure sizes, cannot be directly applied to the fracture originating from the flaw with a microstructure size. Moreover, ceramic materials expected to be of use in engineering ordinarily have polycrystalline structures, which are composed of microscopic grains with individually distinct characteristics such as crystallographic orientation, geometric shape, and size. This implies that various properties of individual grains should be also taken into account as microstructural factors in the strength analysis when the defect is not very large compared with the grain structure. Consequently, the microstructural influences on ceramic strength should be adequately reflected in the *K*-based criterion by investigating detailed stress distribution on the stress field in grains around the crack tip.

In this work, the stress distribution around the crack tip is first numerically analyzed by using a finite element method. In the analysis, the anisotropy appearing in individual grains with distinct crystallographic directions is replaced with the variation of the grain rigidity, and the difference of grain size is dealt with by deforming the shape and size of each element in a divided mesh. A microstructural modification factor for the stress intensity factor *K* is proposed based on the numerical results to take account of the microstructural influences expected in ceramics. Finally, considering the *R*-curve behavior in cracking,[9,10] the strength distribution characteristics are simulated to clarify the influences of microstructural modification factors on the ceramic strength.

2. Modeling and Conditions in Finite Element Analysis

The stress at the crack tip is the focus because this stress is considered to have a direct correlation with the fracture. The crack tip stress is affected by some microstructural factors such as grain size and crystallographic anisotropy of grains around the crack tip. In this analysis, especially, the variations in the grain size and the grain rigidity are examined as dominant microstructural factors.

2.1 Analytical Model

Consider a crack with a total length of $2a$ located at the center of a plate (Fig. 1). A finite element code, MARC (MARC Analysis Research, Palo Alto, CA) is used for the analysis of the elastic stress distribution around the tip of the

Toshihiko Hoshide and **Masahiro Okawa,** Department of Energy Conversion Science, Graduate School of Energy Science, Kyoto University, Sakyo-ku, Kyoto 606-8501, Japan. Contact e-mail: hoshide@energy.kyoto-u.ac.jp.

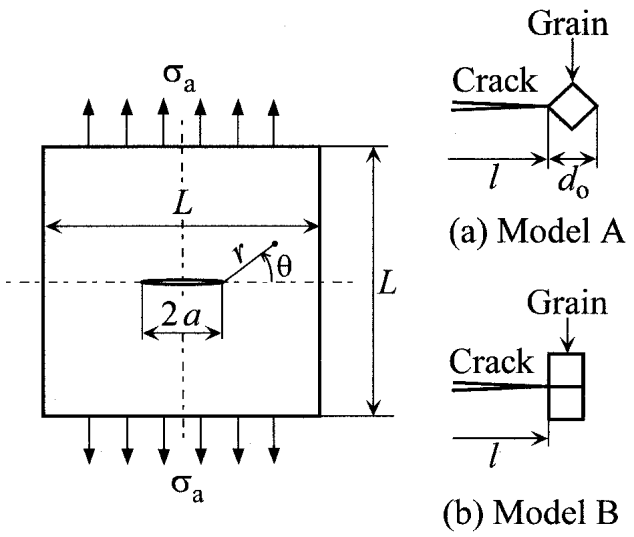

Fig. 1 Center-cracked plate model used in finite element analysis

opening mode crack. In this analysis, one element is assumed as one grain constituting a polycrystalline microstructure, and the half part of the plate is analyzed in consideration of its symmetry (Fig. 1). Although the two models depicted in Fig. 1(a) and (b) have been analyzed for the position of the element at the crack tip (i.e., the crack tip grain), the results obtained using the two models in Fig. 1 are found to be almost the same as in a previous study.[11] Therefore, Model A in Fig. 1(a) is applied to the following simulation.

In the following, an equivalent crack length[2] is introduced to describe the crack length by the formulation including the geometrical effect. Using the half crack length a, an applied stress σ_a, and its related stress intensity factor K, the equivalent crack length l is defined as:

$$l = a\,M^2 = \pi\left(\frac{K}{\sigma_a}\right)^2 \qquad \text{(Eq 1)}$$

In the present model, the stress intensity factor K is evaluated by considering the effect of a finite plate width as follows:

$$K = \sigma_a\sqrt{\pi\,a}\,M \qquad \text{(Eq 2)}$$

The coefficient M is a modification factor for K-estimation associated with the finite width effect and is given by the following modified secant formula[12]:

$$M = [1 - 0.1(a/L)^2 + 0.96(a/L)^4]\,\sqrt{\sec(\pi\,a/L)} \qquad \text{(Eq 3)}$$

The equivalent crack length l implies the length of a virtual crack that provides an identical stress intensity factor in an infinite plate subjected to the uniform applied stress σ_a.

2.2 Modeling of Microstructural Morphology

A material model, which consists of grains with different sizes, is used in the current study. In using a finite element method (FEM), the microstructure is modeled as a two-dimensional area by adopting a regular square element as an initial configuration for the individual grain. As illustrated in Fig. 1(a), the mean grain size d_o is defined as the diagonal of the original regular square element. The original shape of each equilateral square is randomly deformed to represent a more realistic microstructure as follows: four nodes of a square element are moved from their initial positions within a limited circle by using a series of pseudo-uniform random numbers, so that the resultant shape of the square element should be kept convex. For this restriction, the process of making one mesh is repeated five times at most.

In the simulation, the 20 different configurations for FEM mesh are prepared for five kinds of dimensionless crack length $\xi \equiv l/d_o = 0.5$, 1, 2, 5, and 10. This implies that 20 samples with different microstructure configurations are simulated for each crack length.

2.3 Modeling of Crystallographic Direction in Grain

Individual grains in a polycrystalline assembly show different deformation responses because they have distinct crystallographic directions for the principal axial stress direction in a given stress state. To simplify the analytical model, however, a cubic crystal structure is considered as the simplest type of constituent grain, though ceramic materials often have more complex crystal structures (e.g., hexagonal and tetragonal structures). As another simplification, the crystalline anisotropy in the mechanical response is replaced by the difference in grain rigidity, and the rigidity of individual grains (i.e., elements) is also represented by the values of Young's modulus, which are randomly assigned to elements in an FEM analysis.

The elastic constants are assumed to be those for magnesia (MgO) as a model material in this analysis. MgO is a typical ceramic material with a cubic crystal system. Young's modulus E in each crystallographic direction of MgO[13] is as follows: 248.2 GPa in <1 0 0>, 316.4 GPa in <1 1 0>, and 348.9 GPa in <1 1 1>. The mean value $E_o = 298.6$ GPa is obtained from the average of the maximum value 348.9 GPa and the minimum value 248.2 GPa of the material. The maximum and the minimum value of Young's modulus as well as their mean value are adopted for the grain rigidity in the simulation. The three Young's moduli are assigned at random in each mesh element modeled as a grain on condition that the Young's modulus of the grain at the crack tip, E_{tip}, is fixed as one of the three Young's moduli. Independently of Young's modulus, however, the Poisson ratio ν is assumed to be the constant value of 0.17 in the bulk material.

3. Analysis of Influence of Grain Characteristics on Crack Tip Stress

The influences due to the difference of grain rigidity and size on the crack tip stress are analyzed by using the finite element model, which represents more actual microstructures.

3.1 Effect of Grain Rigidity

The crack tip stress is defined as the calculated stress at the center of the grain, which is located at the crack tip. In this analysis, seven grains surrounding the grain at the crack tip are especially focused on, in consideration of the symmetry con-

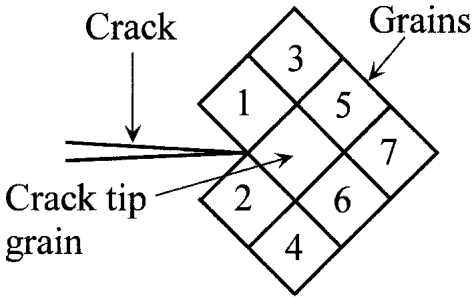

Fig. 2 Numbering of grains around crack tip

cerning the crack. Also, the influences due to the difference in the grain rigidity on the crack tip stress are investigated for each crack length. The Young's moduli of the seven grains are respectively described as E_1, E_2, E_3, E_4, E_5, E_6, and E_7, corresponding to their positions as depicted in Fig. 2. In addition, the following rigidity parameters are introduced using the rigidities of the grains existing at the symmetric positions with respect to the crack line:

$$S_{12} = \frac{(E_1 + E_2)/2}{E_o} \quad \text{(Eq 4a)}$$

$$S_{34} = \frac{(E_3 + E_4)/2}{E_o} \quad \text{(Eq 4b)}$$

$$S_{56} = \frac{(E_5 + E_6)/2}{E_o} \quad \text{(Eq 4c)}$$

$$S_{S7} = \frac{E_7}{E_o} \quad \text{(Eq 4d)}$$

$$S_{T7} = \frac{\left(\sum_{n=1}^{7} E_n\right) \Big/ 7}{E_o} \quad \text{(Eq 4e)}$$

The above parameters are normalized by the mean Young's modulus E_o = 298.6 GPa.

Figure 3 presents the result for ξ = 1 and $E_{tip} = E_o$ as one of analyzed examples. In the figure, the crack tip stress σ is normalized by a stress parameter $\sigma_a \xi^{1/2}$. Figure 3(a) shows the relation of the normalized crack tip stress to the rigidity parameters S_{12} and S_{34}, while the normalized crack tip stress is correlated with the other rigidity parameters S_{56}, S_{S7} and S_{T7} in Fig. 3(b). As seen in Fig. 3(a), the crack tip stress increases with decreasing the grain rigidity parameter S_{12} (see the broken line) and/or increasing the grain rigidity parameter S_{34} (see the dotted line). However, no good correlation is recognized in the relations with the other three parameters S_{56}, S_{S7}, and S_{T7}.

The lower rigidity of grains #1 and #2 makes the crack opening easier, while the higher rigidity of grains #3 and #4 restricts the deformation of the grain at the crack tip. Therefore, the crack tip stress is considered to become greater for the smaller S_{12} and the larger S_{34}. Since the parameters S_{12} and S_{34} show an opposite correlation with the crack tip stress, a specific rigidity parameter S_{12}/S_{34} is expected to better reflect both rigidity effects of the grains around the crack tip. The relation of the crack tip stress to the specific rigidity parameter is plotted in Fig. 4, which indicates a clearer negative interrelationship between them.

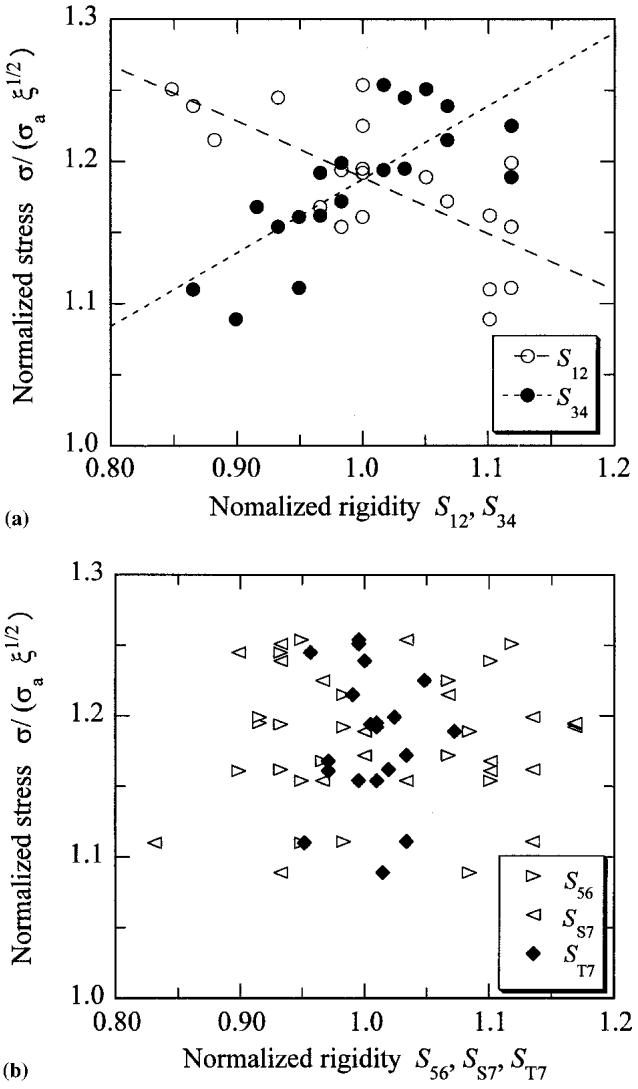

Fig. 3 Relation between normalized stress and normalized rigidity: **(a)** correlations with parameters S_{12} and S_{34}; **(b)** correlations with parameters S_{56}, S_{S7}, and S_{T7}

Similar results are also obtained for the other crack length of ξ = 0.5, 2, 5, and 10, and for other values of the crack tip rigidity E_{tip}. Consequently, it may be concluded that the specific rigidity parameter S_{12}/S_{34} is a dominant parameter representing the grain rigidity effect on the crack tip stress.

3.2 Effect of Grain Size

The relation between the grain size and the crack tip stress is examined in this section. In this analysis, two definitions are considered for the grain size: one is the grain length projected onto the crack line, and another is the square root of the grain area A. No remarkable difference has been found in analyzed results using the two grain size parameters. In the following, therefore, the analyzed results are shown for the grain size defined by using the grain area.

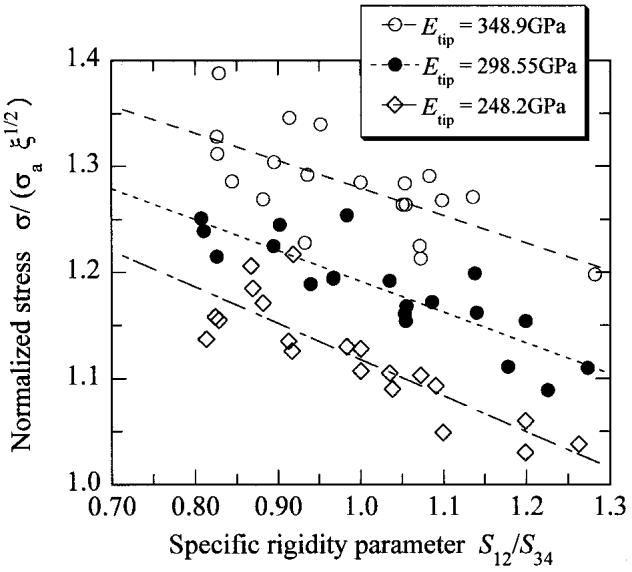

Fig. 4 Normalized stress correlated with specific rigidity parameter

A normalized grain size parameter of the grain at the crack tip is defined by:

$$D_{tip} = \frac{\sqrt{A_{tip}}}{\sqrt{A_{org}}} \quad \text{(Eq 5)}$$

In Eq 5, A_{tip} is the area of the grain at the crack tip, and A_{org} is the area of the element in an original mesh before the initial mesh is deformed. The grain size effect on the crack tip stress is also investigated with respect to grains surrounding the crack tip. Similar to the examination on the grain rigidity effect, the areas of the seven grains around the crack tip are considered. The grain areas are denoted by A_1, A_2, A_3, A_4, A_5, A_6, and A_7, respectively, corresponding to their positions as shown in Fig. 2. Other grain size parameters D with subscripts are defined as follows:

$$D_{12} = \frac{(\sqrt{A_1} + \sqrt{A_2})/2}{\sqrt{A_{org}}} \quad \text{(Eq 6a)}$$

$$D_{34} = \frac{(\sqrt{A_3} + \sqrt{A_4})/2}{\sqrt{A_{org}}} \quad \text{(Eq 6b)}$$

$$D_{56} = \frac{(\sqrt{A_5} + \sqrt{A_6})/2}{\sqrt{A_{org}}} \quad \text{(Eq 6c)}$$

$$D_{S7} = \frac{\sqrt{A_7}}{\sqrt{A_{org}}} \quad \text{(Eq 6d)}$$

$$D_{T7} = \frac{\left(\sum_{n=1}^{7} \sqrt{A_n}\right) \Big/ 7}{\sqrt{A_{org}}} \quad \text{(Eq 6e)}$$

Figure 5 presents the result for $\xi = 1$ and $E_{tip} = E_o$ as one of the analyzed examples. The normalized crack tip stress is correlated with the grain size parameters D_{tip}, D_{12}, and D_{34} in Fig. 5(a), and also D_{56}, D_{S7}, and D_{T7} in Fig. 5(b). As indicated in Fig. 5, any grain size parameter has no significant interrelation with the crack tip stress. Similar results are also found for the other crack length of $\xi = 0.5$, 2, 5, and 10, and for other values of the crack tip rigidity E_{tip}.

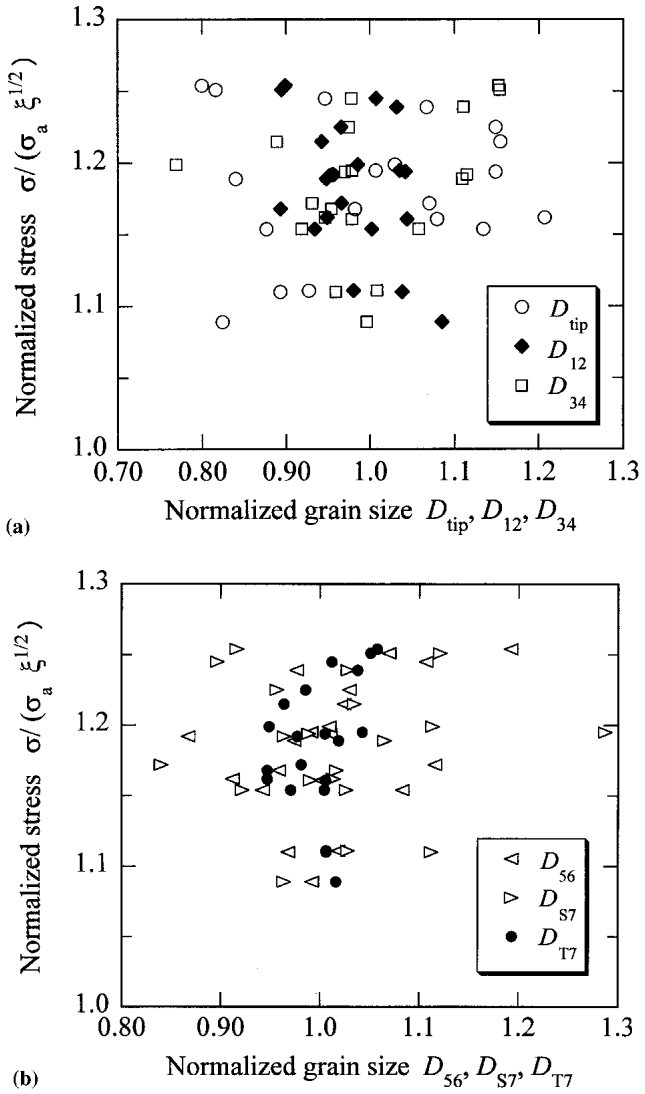

Fig. 5 Relation between normalized stress and normalized grain size: **(a)** correlations with parameters D_{tip}, D_{12}, and D_{34}; **(b)** correlations with parameters D_{56}, D_{S7}, and D_{T7}

Therefore, note that the grain size of any grain at and around the crack tip does not have a strong influence on the crack tip stress, especially compared with the effect of the grain rigidity.

4. Microstructural Modification Factor of Stress Intensity Factor for Crack of Microstructure Order

4.1 Definition of Microstructural Modification Factor

Using the polar coordinate system (r, θ) with its origin at the crack tip, the distribution of stress σ_y in the direction vertical to the crack is expressed as the following stress singularity form:

$$\sigma_{y,\mathrm{SIF}} = \frac{K}{\sqrt{2\pi r}} \cos\frac{\theta}{2}\left(1 + \sin\frac{\theta}{2}\sin\frac{3\theta}{2}\right) \quad \text{(Eq 7)}$$

where r is the distance from the crack tip and θ is the angle measured from the crack line counterclockwise (Fig. 1). If the stress intensity factor is used for the fracture problem associated with the crack of the microstructure order, a modification is required to evaluate the stress intensity factor by using a new modification factor f_M to reflect the microstructural effect. In this case, a modified stress intensity factor is expressed as:

$$K = \sigma_a \sqrt{\pi l}\, f_M \quad \text{(Eq 8)}$$

where the equivalent crack length l defined in Eq 1 is used. The factor f_M is called the microstructural modification factor in the following. When the stress $\sigma_{y,\mathrm{FEM}}$ in the element at the crack tip is given as the crack tip stress obtained by the aforementioned FEM analysis, the microstructural modification factor f_M is defined by the following equation:

$$f_M = \frac{\sigma_{y,\mathrm{FEM}}}{\sigma_{y,\mathrm{SIF}}} \quad \text{(Eq 9)}$$

The value of $\sigma_{y,\mathrm{SIF}}$ is uniquely determined for a given crack length by setting $\theta = 0$ and $r = d_o/2$ in Eq 7 for the present model as depicted in Fig. 1(a). On the other hand, even for the same crack length, the crack tip stress $\sigma_{y,\mathrm{FEM}}$ changes due to the variation in modeled microstructure configuration with different combinations of grain rigidity and size. Consequently, the microstructural modification factor f_M may also have distinct values even though the crack length is given.

4.2 Distribution Characteristics of Microstructural Modification Factor

The distribution characteristics of the microstructural modification factor f_M defined in the previous section is investigated using the Weibull distribution function:

$$F(f_M) = 1 - \exp\left[-\left(\frac{f_M - \gamma}{\beta}\right)^{\alpha}\right] \quad \text{(Eq 10)}$$

where $F(f_M)$ is the cumulative probability of f_M, and α, β, and γ are the shape, scale, and location parameters, respectively.

Figure 6 shows the distribution of f_M plotted on a Weibull probability paper. The straight lines in the figure represent the regression lines when the f_M distributions are fitted to the two-parameter Weibull distribution functions set as $\gamma = 0$ in Eq 10. As seen in Fig. 6, the f_M distribution for a longer crack shifts toward a lower side. No significant difference is seen between the f_M distributions in the cases of $\xi = 5$ and $\xi = 10$. This suggests an asymptotic behavior of the f_M distribution to a specific distribution for the crack length, which is long enough. In Table 1, the shape and scale parameters in the fitted Weibull distribution function are summarized. Table 1 shows that the shape parameter is almost the same independently of the crack length. This implies that the relative scatter of the f_M value hardly varies as the crack length is changed.

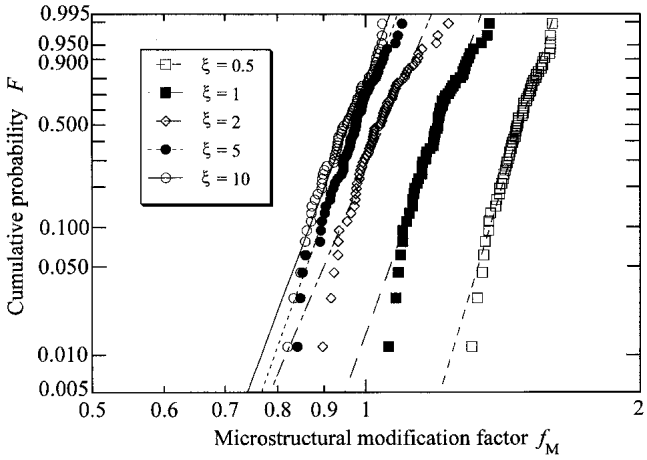

Fig. 6 Distribution of f_M-value plotted on Weibull probability paper

Table 1 Parameters in Two-Parameter Weibull Function Fitted to f_M Distribution

$\zeta = l/d_o$	Shape Parameter α	Scale Parameter β
0.5	25.0	1.50
1	21.5	1.23
2	18.4	1.07
5	20.6	0.998
10	19.9	0.975

5. Strength Distribution Characteristics Including Microstructural Effects

5.1 Fracture Criterion for Small Crack

The brittle fracture criterion based on the stress intensity factor K is ordinarily expressed by

$$K = K_{\mathrm{IC}} \quad \text{(Eq 11)}$$

where K_{IC} is the plane-strain fracture toughness. However, for the ceramic fracture initiated from an inherent flaw of the microstructure size, the fracture criterion should be modified by using the microstructural modification factor f_M as follows:

$$K_{f_M} = K_{\mathrm{IC}} \quad \text{(Eq 12)}$$

In addition, it is recognized that the crack growth resistance K_C in ceramic materials changes mainly due to the grain bridging, which depends on the crack length. Therefore, the criterion of Eq 12 should be further replaced with

$$K_{f_M} = K_C \quad \text{(Eq 13)}$$

The concept of R-curve is introduced in the analysis, and its detail is described in the next section.

5.2 R-Curve Model to Be Used in Simulation

In most engineering ceramics, the surface free energy in a single crystal is generally smaller than the effective surface

energy required for unstable cracking in polycrystalline materials.[14-16] The higher energy in a polycrystal is attributed to a much rougher fracture surface compared with that in a single crystal, because the fracture surface area is larger due to a rougher cracking path. In this situation, *R*-curve behavior is expected to appear.

To express the grain bridging effect in ceramics, particularly, Mai et al.[9,10] proposed *R*-curve formulations. However, when the *R*-curve expression proposed by Mai and Lawn is applied, an anomalous behavior is observed[11] in the crack length versus strength relation as follows. The strength decreases steadily with increasing crack length in the region of $\xi < 1$, increases for a time as ξ exceeds unity, and decreases again after the increase in strength. This result is suggested to be caused by using the *R*-curve formulation proposed by Mai and Lawn.[9] To solve the problem and to simplify the formulation, a new *R*-curve expression of an exponential type has been proposed elsewhere.[11] In this work, the exponential type *R*-curve as described below is adopted for the fracture criterion:

$$K_C = K_{CO} = K_{IC}\,[1 - R_O \exp(-C)] \text{ for } \xi \leq 1 \quad \text{(Eq 14a)}$$

$$K_C = K_{IC}\,[1 - R_O \exp(-C\xi^n)] \text{ for } \xi > 1 \quad \text{(Eq 14b)}$$

where K_{CO}, R_O, C, and n are constants. Defining $R_{CO} \equiv K_{CO}/K_{IC}$, the following relation is obtained:

$$R_O = (1 - R_{CO}) \exp(C) \quad \text{(Eq 15)}$$

The above expression is more easily dealt with in its application compared with the Mai-Lawn model. In another work,[11] it is found that the parameters $C = 0.8$, $n = 0.5$, and $R_{CO} = 0.61$ are appropriate for Eq 14 as the approximation for the Mai-Lawn model.

5.3 Estimation of Strength Distribution

In this section, the strength distribution in ceramics is estimated based on the aforementioned discussions. Using the equivalent crack length l, the microstructural modification factor f_M, and the *R*-curve concept, the fracture criterion given by Eq 13 is rewritten as the following criterion including the fracture strength σ_f:

$$(\sigma_f \sqrt{\pi l})\, f_M = K_C \quad \text{(Eq 16)}$$

Equation 16 yields the expression for σ_f as follows:

$$\sigma_f = \frac{K_C}{\sqrt{\pi\, l}\, f_M} \quad \text{(Eq 17)}$$

It can be understood that the strength σ_f shows dispersion by the variation of the microstructural modification factor f_M. Therefore, if the variation of the microstructural modification factor f_M is specified, the strength distribution in ceramics can be evaluated. The distribution of f_M has been derived by stress analysis using finite element analysis and can be approximated by the two-parameter Weibull distribution function with $\gamma = 0$ in Eq 10. Using the cumulative probability F as a random variable, Eq 10 gives f_M as a function of F as follows:

$$f_M = \exp\left[\frac{1}{\alpha} \ln\{-\ln(1 - F)\} + \ln \beta\right] \quad \text{(Eq 18)}$$

The strength distribution can be evaluated by Eq 17 with Eq 18. In addition, Eq 14 of the *R*-curve expression is substituted into K_C in Eq 17, and the normalized fracture strength $\Sigma_f = \sigma_f / [K_{IC} / (\pi\, d_o)^{1/2}]$ is obtained by:

$$\sum\nolimits_f = \frac{1 - R_O \exp(-C)}{\sqrt{\xi} \exp[\ln\{-\ln(1 - F)\}/\alpha + \ln \beta]} \text{ for } \xi \leq 1 \quad \text{(Eq 19a)}$$

$$\sum\nolimits_f = \frac{1 - R_O \exp(-C\xi^n)}{\sqrt{\xi} \exp[\ln\{-\ln(1 - F)\}/\alpha + \ln \beta]} \text{ for } \xi > 1 \quad \text{(Eq 19b)}$$

In this estimation, the upper and lower bounds of the normalized strength are respectively calculated by substituting $F = 0.999$ and $F = 0.001$ into Eq 19 for five discrete values of the normalized crack length ξ. Scatter bands of the normalized strength obtained by the calculation are indicated with the solid curves in Fig. 7. For reference, experimental results [2,5,17,18] for several ceramic materials (Table 2) are pooled, and also plotted with circle marks in Fig. 7. The estimated scatter band expresses the central trend of dispersed experimental results. Although the calculated dispersion of strength is narrower compared with the scatter in experiments, note that experimen-

Table 2 Mechanical Properties of Ceramic Materials as Reference Data

Material	Bulk Density ρ, Mg/m^3	Young's Modulus E-GPa	Mean Grain Size d_o-μm	Fracture Toughness K_{IC}, MPa · m$^{1/2}$	Mean Strength σ_f, MPa
Alumina, AL-1	3.93	380	5.3	4.4	381 (a)
Alumina, 96%	3.7	349	10	3.6	414 (b)
Alumina, 92%	3.6	290	20	3.2	302 (b)
Silicon nitride, EC-141	3.23	320	1.6	6.0	1060 (a)
Silicon nitride, EC-1211	3.26	330	5.0	5.7	834 (b)
					800 (c)
Sialon	3.22	294	2.1	5.8	788 (c)
Zirconia, PSZ	6.0	218	1.0	6.0	1126 (b)

Loading mode in strength test: (a) four-point bending, (b) three-point bending, (c) ring compression

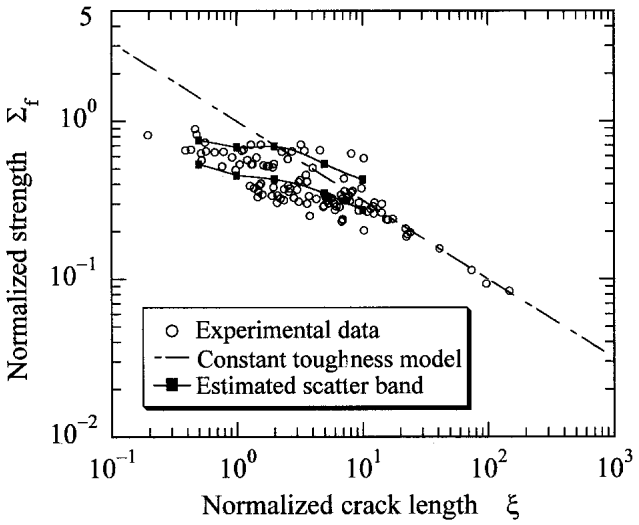

Fig. 7 Relation between normalized strength and normalized crack length

tal results are pooled for several ceramics with different mechanical properties, and the *R*-curve property may have a scatter, too.

6. Summary

A numerical analysis of the stress distribution around the crack tip was conducted by using an FEM, in which each element was regarded as one grain constituting a material microstructure. In the FEM model, the anisotropy appearing in individual grains with distinct crystallographic directions was replaced with the variation of the grain rigidity, and the difference of grain size was dealt with by deforming the shape and size of each original square element in an initially divided mesh.

As for the grain rigidity, the crack tip stress was well correlated with the parameters using Young's moduli of the grains just behind the crack tip and also the grains above and below the grain at the crack tip. It was found that the crack tip stress was higher for a lower rigidity of the grains just behind the crack tip and/or for a higher rigidity of the grains above and below the grain at the crack tip. However, the size of grains at and around the crack tip hardly affected the crack tip stress compared with the effect of the grain rigidity

A modification factor for the stress intensity factor *K* was proposed based on the numerical results to take account of the microstructural influences expected in ceramics. In this study, the microstructural modification factor f_M was defined as the ratio of the stress in the crack tip element, which was calculated by the FEM analysis, divided by the *K*-based stress. The statistical properties of obtained f_M values were investigated in the Weibull plots. The f_M distributions were fitted to the two-parameter Weibull distribution function. The f_M distribution for a longer crack was found to shift toward a lower side. It was also suggested that an asymptotic behavior of the f_M distribution to a specific distribution appeared with increasing the crack length. On the other hand, the scatter of the f_M value was almost the same for different crack lengths.

In the strength analysis, the fracture criterion was modified by using the microstructural modification factor f_M for the ceramic fracture originating from an inherent flaw in microstructure size. In addition, by including the *R*-curve effect in the criterion, the strength distribution characteristics were simulated to clarify the influences of microstructural factors on the ceramic strength. To express the grain bridging effect in ceramics, the *R*-curve expression of an exponential type was applied in the simulation. It was found that the estimated scatter band in the relation between the strength and the crack length represented the central trend of dispersed experimental results.

References

1. A.G. Evans and T.G. Langdon: "Structural Ceramics," *Prog. Mater. Sci*., 1976, *21*, pp. 191-93.
2. T. Hoshide, H. Furuya, Y. Nagase, and T. Yamada: "Fracture Mechanics Approach to Evaluation of Strength in Sintered Silicon Nitride," *Int. J. Fract.,* 1984, *26*, pp. 229-39.
3. S. Usami, H. Kimoto, I. Takahashi, and S. Shida: "Strength of Ceramic Materials Containing Small Flaw," *Eng. Fract. Mech.,* 1986, *23*(4), pp. 745-61.
4. T. Yamada: "Behaviour of Cyclic Fatigue Strength and Inherent Flaws of Ceramics" in *Proc. 31st Symp. Mater. Strength Fract.,* 1986, *31*, pp. 51-63.
5. J. Kitazumi, Y. Taniguchi, T. Hoshide, and T. Yamada: "Characteristics of Strength and Their Relations to Flaw Size Distribution in Several Ceramic Materials: Part 1, Static Strength," *J. Soc. Mater. Sci.,* Japan, 1989, *38*(434), pp. 1254-60 (in Japanese).
6. K. Tanaka, K. Suzuki, and Y. Yamamoto: "Residual-Stress Effect on Fracture Strength of Ceramics" in *Proc. Int. Conf. Residual Stresses (ICRS2),* G. Beck, S. Denis, and A. Simon, ed., Elsevier Applied Science, London and New York, 1989, pp. 15-26.
7. T. Hoshide and T. Inoue: "Simulation of Anomalous Behavior of a Small Flaw in Strength of Engineering Ceramics," *Eng. Fract. Mech.,* 1991, *38*(4/5), pp. 307-12.
8. T. Hoshide: "Grain Fracture Model and Its Application to Strength Evaluation in Engineering Ceramics," *Eng. Fract. Mech.,* 1993, *44*(3), pp. 403-08.
9. Y.-W. Mai and B.R. Lawn: "Crack-Interface Grain Bridging as a Fracture Resistance Mechanism in Ceramics: II, Theoretical Fracture Mechanics Model," *J. Am. Ceram. Soc.,* 1987, *70*(4), pp. 289-94.
10. R.F. Cook, C.J. Fairbanks, B.R. Lawn, and Y.-M. Mai: "Crack Resistance by Interfacial Bridging: Its Role in Determining Strength Characteristics," *J. Mater. Res.,* 1987, *2*(3), pp. 345-56.
11. T. Hoshide and H. Hiramatsu: "A Microstructural Approach to Flaw Size Dependence of Strength in Engineering Ceramics," *Fatigue Fract. Eng. Mater. Struct*., 1999, *22*, pp. 1029-39.
12. H. Tada: "A Note on the Finite Width Corrections to the Stress Intensity Factor," *Eng. Fract. Mech.,* 1971, *3*(3), pp. 345-47.
13. R.W. Davidge: *Mechanical Behaviour of Ceramics*, Cambridge University Press, Cambridge, 1979, p. 22.
14. J.P. Singh, A.V. Virkar, D.K. Shetty, and R.S. Gordon: "Strength-Grain Size Relations in Polycrystalline Ceramics," *J. Am. Ceram. Soc.,* 1979, *62*(3-4), pp. 179-83.
15. R.W. Rice, S.W. Freiman, and J.J. Mecholsky, Jr.: "The Dependence of Strength-Controlling Fracture Energy on the Flaw-Size to Grain-Size Ratio," *J. Am. Ceram. Soc.,* 1980, *63*(3), pp. 129-36.
16. R.W. Rice, S.W. Freiman, and P.F. Becher: "Grain-Size Dependence of Fracture Energy in Ceramics: I, Experiments," *J. Am. Ceram. Soc.,* 1981, *64*(6), pp. 345-50.
17. J. Kitazumi, Y. Taniguchi, and T. Yamada: "Fatigue Strength of Sialon in Ring Compression Tests," *The Memoirs of the Niihama National College of Technology (Science and Engineering),* 1988, *24*, pp. 9-14 (in Japanese).
18. T. Hoshide and M. Masuda: "Dependence of Strength on Size of Flaw Dominating Fracture in Ceramics," *Mater. Sci. Res. Int.,* 1995, *1*(2), pp. 108-13.